Preprint typeset in JINST style - HYPER VERSION

CALICE Analysis Note CAN-037
30th November 2012

First results of the CALICE SDHCAL technological prototype

CALICE collaboration*

This note contains preliminary CALICE results, and is for the use of members of the CALICE Collaboration and others to whom permission has been given.

ABSTRACT: The CALICE Semi-Digital Hadronic CALorimeter (SDHCAL) prototype, built in 2011, was exposed to beams of pions, electrons and muons at CERN in two periods of two weeks each in 2012. The prototype with its 48 active layers was run using the triggerless and power-pulsing modes. The performances of the SDHCAL during the test beam were found to be very satisfactory with efficiency exceeding 90% for almost all of the 48 Glass Resistive Plate Chambers (GRPC). The preliminary results show that by using appropriate calibration coefficients, a linear response (within 4%) and a good energy resolution are obtained for a large range of hadronic energies (10–80 GeV) for both the Digital (Binary) and the Semi-Digital (Multi-threshold) modes of the SDHCAL prototype.

*Corresponding author: G. Grenier (grenier@ipnl.in2p3.fr)

Contents

1. Introduction

The SDHCAL prototype was conceived for two purposes. The first one is to confirm that highly-granular gaseous hadronic calorimeters are capable of achieving good resolution of the hadronic energy measurement while providing an excellent tracking tool for the Particle Flow Algorithms (PFA). The second and most important aim is to demonstrate that such calorimeters are compatible with the requirements of future ILC experiments in terms of efficiency, compactness and low power consumption.

In the following, after a short description of the prototype and of the beams used to test it, the event building procedure and the data quality will be presented in the second section. In section 3, particle identification will be discussed, and hadronic shower selection will be detailed. In section 4 the linearity and resolution of the hadronic shower energy reconstruction will be presented.

1.1 Prototype description

The SDHCAL comprises 48 active layers. Each of these layers is made of 1 m^2 Glass Resistive Plate Chamber (GRPC). The GRPC signal is read out through 9216 pads of 1 cm^2 each. The pads are located on one face of an electronics board which hosts 144 HARDROC ASICs [1] on its other side. Each electronics board is built by soldering three slabs covering each a third of the detector surface. The GRPC and the electronics board are put inside a cassette made of two stainless steel walls of 2.5 mm thickness each. The cassette keeps the pick-up pads of the electronics board in contact with the GRPC, and, it constitutes a part of the calorimeter absorber. The total thickness of a cassette is 11 mm of which 6 mm are the active layer thickness occupied by the GRPC (3 mm), and the readout electronics (3 mm). A cross-section of the active layer inside the cassette is shown in Fig. 1.

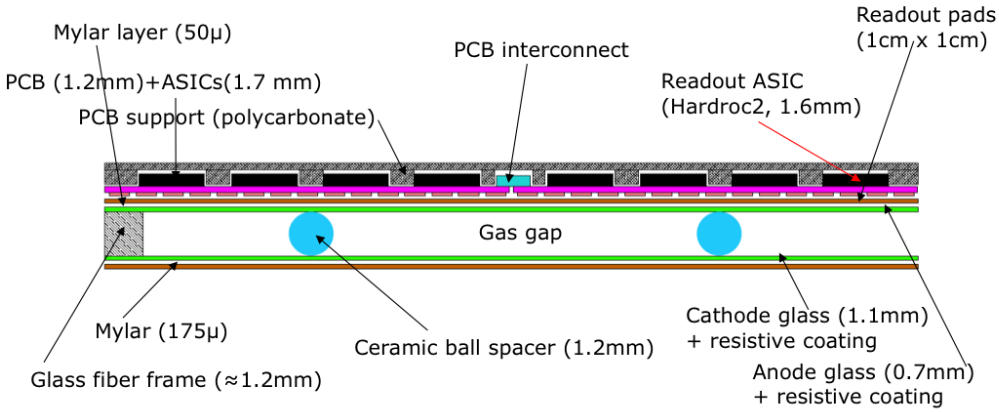

Figure 1. A schematic cross-section of the active layer inside a SDHCAL cassette.

The upper part of the cassette hosts also three Detector InterFace (DIF) cards which transfer the acquisition commands received through HDMI cables to the ASICs of each slab, and collect the data received from these ASICs before forwarding the data through USB protocol to the acquisition stations.

The 48 cassettes are then inserted into a self-supporting mechanical structure. The structure is built using 1.5 cm thickness stainless steel plates with a distance of 13 mm between two consecutive plates to allow an easy insertion of the cassettes. A SDHCAL layer made of one cassette and 1.5 cm thickness stainless steel plates corresponds to 0.12 interaction length. The acquisition mode used in the test beam (TB) was the triggerless mode. In this mode, data are collected after an acquisition command is sent to the ASIC. When the memory of one ASIC is full, a RamFull command is sent to all, and the acquisition is stopped to allow the readout of the data recorded in the different ASICs. The acquisition restarts automatically upon the completion of the data transfer. During the data transfer no data is collected. This dead time was reduced by increasing the number of USB buses for the data transfer.

The heating due to the power consumption of more than 440 000 channels of the prototype leads ineluctably to an increase of the prototype temperature which results in a change of the GRPC

gain and an increase of the noise. Although the GRPC gain can be controlled to some extent by reducing the high voltage applied to the GRPC, the noise could not be reduced easily. To avoid these problems the power-pulsing mode was used. This mode allows to keep the electronics in an idle mode during the time period separating two beam spills. In the case of the SPS beam cycle this amounts to a reduction factor of five of the ASIC consumption (about nine seconds spill duration within a cycle of approximately 45 s). To further reduce the heating effect, a simple cooling system was used. It is made of two cassettes made of copper, and put in contact with the two lateral sides of the calorimeter. A water circuit is installed into the two cassettes, and the water temperature is maintained at 10°C. In addition a dry air distribution system was used to eliminate the effect of the DIF heating on the cassettes.

1.2 CERN SPS beam data samples

The SDHCAL prototype was exposed to pions, muons and electrons of the CERN H2 beam line of the SPS in May, and of the H6 beam line in August. Since the GRPC efficiency decreases at high particle rate [2] the optics was set up to enlarge the beam size, and have it as flat as possible while reducing its intensity. This allowed to reach the optimal GRPC efficiency, and at the same time to collect as much statistics as possible. To control the beam intensity in an independent way the efficiency of the muons as well as the pion track segment before it showers[1] was monitored online. Consequently, only runs with particle rates smaller than 1000 particles/spill (i.e. less than 100 Hz/cm^2) were found to satisfy the performance requirements. During the May and August beam tests several energy points were studied. Pions of 20, 30, 40, 50, 60, 70 and 80 GeV and electrons of 10, 20, 30, 40, 50 and 60 GeV were studied in the May beam test. More energy points were covered in August for pions : 5, 7.5, 10, 15, 20, 25, 30, 40, 50, 60, 70, 80, 90, 100 GeV. Only few dedicated muons runs were taken. The pion and electron runs contain indeed an important contribution of muons resulting essentially from pions stopped in the collimators. To reduce the electron contamination of pion runs, a 4 mm lead target was used. The use of this target was found to be rather effective at high energy (E > 20 GeV). At lower energies a significant contamination is observed. Positive pions were used in this study. It is well known that the contamination of these pions by protons is rather high at energy above 20 GeV [3]. This should not be an obstacle to study the SDHCAL performance since at these energies one does not expect sizable differences in the behavior of the hadronic showers produced by both species.

1.3 Prototype running operation

An important feature of the SDHCAL readout is the presence of three thresholds. The aim of using the thresholds information is not to measure the energy deposit in each pad but an attempt to distinguish between pads crossed by few, many or too many charged particles. Information of three thresholds is coded in two bits. The thresholds values were fixed to 114 fC, 5 pC and 15 pC respectively, the average MIP induced charge being around 1.2 pC. The choice of these values was motivated by simulation studies. These values will eventually be optimized by dedicated studies in future test beams. During the May run one slab on the lateral position of chamber number 46 was

[1] The method to estimate the efficiency will be presented in section 2.

out of order, and kept off all the time. This was repaired for the August run. However, only the first 47 layers were active in the first part of the August run.

In addition seven ASICs were switched off. Three of them failed during the preparation tests in the laboratory, and were not replaced. Four additional ASICs were found noisy and were masked. This represents about one per mil of the total number of channels. No additional ASIC died during the data taking, or between the two test beam periods.

For the May and August runs of 2012 no gain correction was applied. The same electronics gain was used for all the channels (g=1). This was done in order to see the performance that this technology can reach without any correction.

The gas mixture used to run the GRPC was made of TetraFluoroEthane (TFE, 93 %), CO_2 (5 %) and SF_6 (2 %). The high voltage applied on the GRPC was of 6.9 kV.

2. Event building and data quality control

With the use of the triggerless acquisition mode in the 2012 runs, collected data include not only the information of the fired pads (hits) resulting from the interaction of the beam particles (pions, electrons, muons, ...) but also those due to cosmic rays and the noise-related ones. To select hits related to the incoming beam particles, a time clustering procedure is used. The time occurrence of the hits is recorded using a time-stamp whose counter is incremented by a step of 200 ns (the ASIC internal clock period).

A histogram of hit time occurrence is built for each acquisition readout (Fig. 2) with a bin-width set to the time-stamp precision. This includes noise, 40 GeV pion events and muons from the beam as well as cosmic rays. Only clock ticks with a number of hits higher than seven are then used to initiate the time clustering process. This choice allows to reject noise events while eliminating negligible fraction of hadronic showers produced by pions of energy larger than 5 GeV. Hits belonging to a local maximum as well as those of the two adjacent clock ticks are gathered to build a physics event. No hit can belong to two different events. The choice of the three adjacent clock ticks to build an event is the result of a dedicated study using cosmic rays. Beside the time occurrence the only information to be used in the following analysis are the space coordinates of the hits determined by the location of the fired pad and the cassette to which it belongs, and the thresholds coding (either 1, 2 or 3).

Among the selected events there are few which are clearly due to electronics noise (Fig. 3). These events are characterized by the occurrence of many hits belonging to the same electronics slab, and sometimes to the whole electronics board made of three slabs. Those coherent-noise events are easily identified since the hits are concentrated in one layer. They have a topology that is completely different from a particle interaction in the calorimeter. Those events which are probably related to grounding problems in some layers were removed from the selection. Once the hits of the physical events and the ones associated to the coherent noise are singled out the remaining hits are used to estimate the noise rate. Figure 4 shows a distribution of the number of noise hits recorded by the entire prototype between two ASIC clock ticks (a time slot of 200 ns). From this distribution, one can estimate the number of noise hits in one physical event (three clock ticks) to be around one hit. This is a rather negligible number, and is much less than the statistical fluctuation of the number of hits of a hadronic shower at energies above 5 GeV.

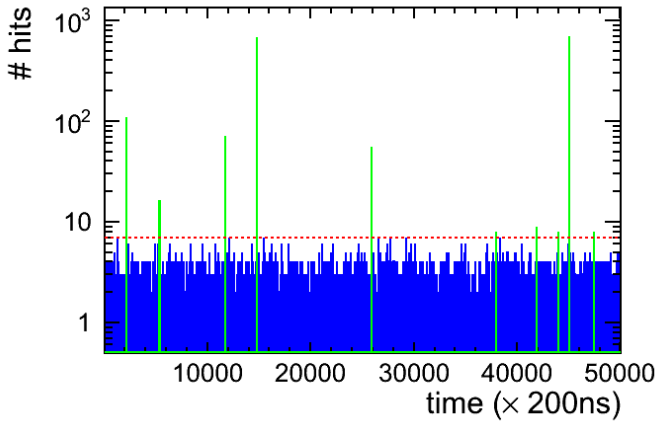

Figure 2. Hit time spectrum for a 40 GeV pion beam run. Each bin corresponds to one clock tick of the detector's electronics (200 ns). The green lines show the physics events selected by time clusterisation, i.e. events above the red dashed line.

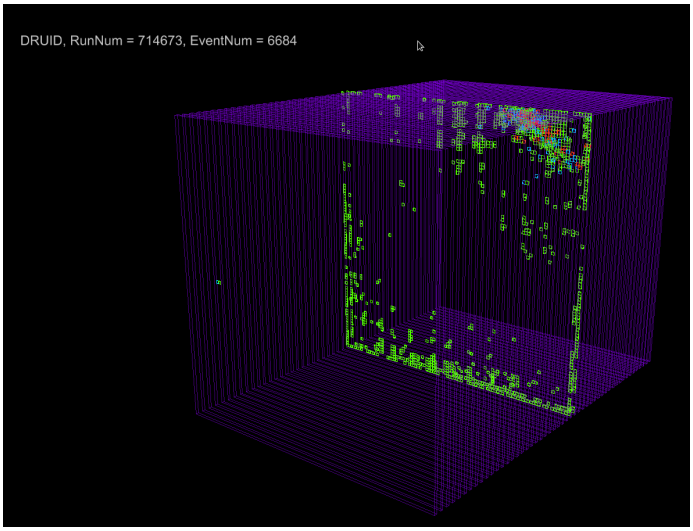

Figure 3. Example of a coherent noise events display.

To monitor the calorimeter performance, the efficiency and particle multiplicity of each of the 48 layers are estimated using the beam muons. To study the efficiency of one layer, tracks are built using the hits of the other layers. To build a track, hits of each layer are grouped in clusters if they share an edge. Isolated clusters which are at least 12 cm away from other clusters of the same layer but also of those of other layers are dropped. Tracks are then built from all the selected clusters excluding the layer under study. Tracks are required to have clusters in at least seven layers. The layers should be on the two sides of the studied layer except of course for the first and last layer.

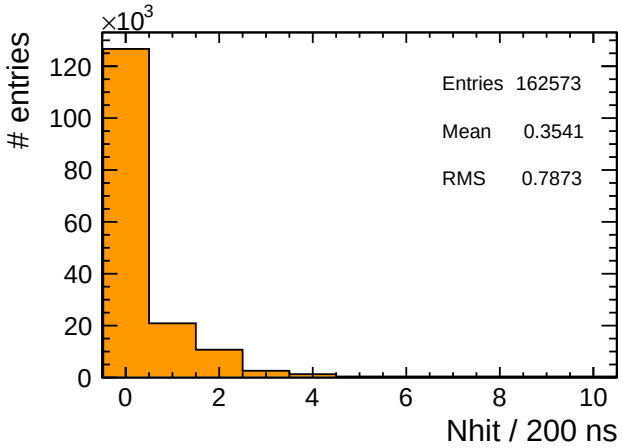

Figure 4. Distribution of the number of noise hits in a time slot of 200 ns (one clock tick) for the whole detector. An average of 0.35 hits / 200 ns is found for the complete detector.

The χ^2 of the constructed track is then estimated[2]. Only tracks with a $\chi^2 < 20$ are used. The expected impact point of the track in the layer under study is determined. The efficiency is then estimated as being the fraction of tracks for which at least one hit is found at a distance of less than 3 cm around the expected position. A track by track multiplicity is also estimated by counting the number of hits, if any, in the cluster built around the closest hit to the track's impact. A particle multiplicity for one sensitive region of the detector is then computed by averaging the track by track multiplicity for tracks going through the sensitive region under study. Figure 5 shows the efficiency and particle multiplicity of the layers during the August 2012 run. Other methods to estimate the efficiency and particle multiplicity were performed, and confirm the results presented here.

3. Particle identification

3.1 Topological variables

To study the hadronic showers, and reconstruct their energy, a selection based on topological characteristics is applied to single out the pions. Different topological variables are used. The variables are computed using all the hits of a given event, or the clusters built from these hits.

Using a lead absorber of 4 mm thickness, the contamination of our data with electrons is expected to be negligible, which is true for beam energies of 20 GeV and more. The contamination is less negligible for beam energies below 20 GeV, and quite important when the beam energy is below 10 GeV. Beam muons and muons from cosmic rays are the main contamination of our pion sample. To distinguish events produced by beam muons and cosmics from those produced by pions the Principal Component method was used [4]. The event's principal axes are computed. These axes which correspond to the three eigenvalues $(\lambda_1, \lambda_2, \lambda_3)$ are sorted in increasing order $(\lambda_1 < \lambda_2 < \lambda_3)$. The ratio of lowest and largest values are used to distinguish muon shapes (small

[2]The cluster x (resp. y) position error used to compute the χ^2 is taken as $N_h/\sqrt{12}$ cm where N_h is the number of cluster's hits projected on the x (resp. y) axis.

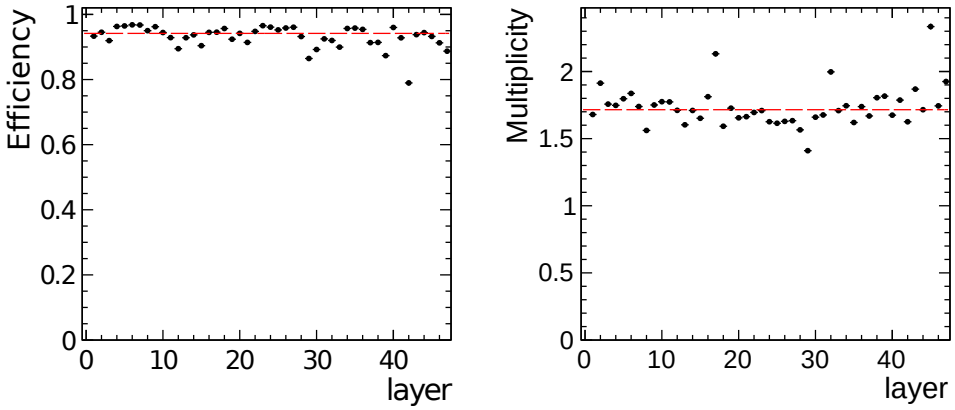

Figure 5. Efficiency (left) and particle multiplicity (right) of the 47 layers used in August run. The red line is the average efficiency (left) and average multiplicity (right).

ratio) from electrons and pions. The three λ_i are the standard deviation of the projection of the hit spatial distribution on three axes. For λ_3, the projection axis is the one which maximizes the standard deviation of the projection. For λ_2, the axis is the one that maximizes the standard deviation of the projection with the constraint to be orthogonal to the axis defining λ_3. λ_1 is the standard deviation of the projected distribution on the axis orthogonal to the two axes defining λ_2 and λ_3. Thus λ_3 measures the longitudinal extent of the shower while λ_1 and λ_2 measure the shower lateral extent. In the same way two principal axes $(\lambda_{1\mathrm{p}}, \lambda_{2\mathrm{p}})$ are defined for each layer. In addition to these two axes the hits barycenter of each layer is also determined.

To further purify the sample, and eliminate the contamination from electrons, additional variables are introduced. For the first variable, N_{25}^{layer}, the number of hits in the 5×5 pads around the barycenter within each layer is computed for each layer. These numbers are then summed over all layers: $N_{25} = \sum_{layer} N_{25}^{layer}$. The first variable V_1 is then defined as the ratio of this sum to the total number of hits in the detector:

$$V_1 = \frac{N_{25}}{N_{\mathrm{hit}}}$$

The value of V_1 in electron-induced shower is expected to be greater than those for pion ones.

The second variable exploits also the shape difference between showers produced by electrons, and those produced by pions, and it is obtained by computing a box-counting fractal dimension. The variable uses the 3-D fractal dimension variable $\mathrm{FD_{3D}}$ which is a 3-D extension of the 2-D one given in [5], and it is defined as:

$$\mathrm{FD_{3D}} = \frac{1}{|I|} \sum_{n \in I} \frac{\ln(N_{\mathrm{hit}}/N_{\mathrm{cube}}(n))}{\ln(n)}$$

where N_{hit} is the total number of hits, $N_{\mathrm{cube}}(n)$ is the number of cubes containing $n \times n \times n$ pads with at least one hit, and I is the set of the different values of n used to build $\mathrm{FD_{3D}}$: $I = \{2,3,4,6,8,12,16\}$, and $|I| = 7$ (here) its cardinality.

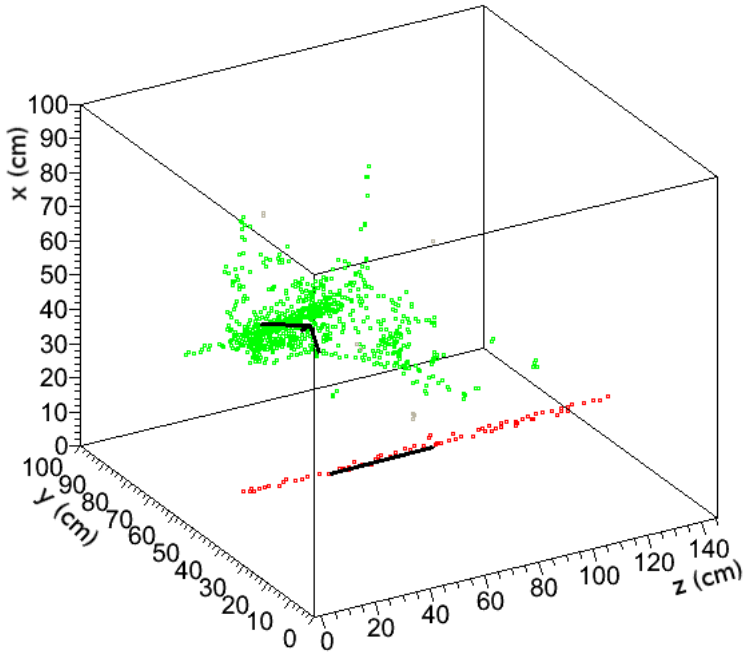

Figure 6. Interaction of a 50 GeV pion and a muon from the beam in the SDHCAL. The pion and the muon are in the same event. Green and red hits are two reconstructed showers. One shower obviously corresponds to a muon. A few hits unassociated with a shower are shown in gray. Principal axes are drawn for the two reconstructed showers with a length corresponding to the eigenvalues λ_i. The λ_2 and λ_3 values for the muon are so small that they are not visible on the display. Their smallness will be used to reject them in the analysis.

The choice of these n values in our case is suggested by the number of pads in one plane (96×96), and the number of layers (48). The compact shape of the electromagnetic shower favors low value of $\mathrm{FD_{3D}}$ with respect to pions of the same energy. In order to discriminate electrons and pions of different energy the variable $V_2 = \mathrm{FD_{3D}}/\ln(N_{\mathrm{hit}})$ is introduced.

The planes following interactions of a pion/electron with the absorber material can be characterized by looking at the distribution of hits within each plane. Those who contain the hadronic/electromagnetic shower are called interaction planes here after. To recognize these planes we ask that their principal axes $\lambda_{1\mathrm{p}}$ and $\lambda_{2\mathrm{p}}$ satisfy $\sqrt{\lambda_{1\mathrm{p}}^2 + \lambda_{2\mathrm{p}}^2} > 1.5$ cm, or their number of hits is greater than five. The planes where the hadronic/electromagnetic shower is potentially developing are called shower planes. The shower planes are the first interaction plane, the last interaction plane and all those located in between.

3.2 Shower reconstruction and first selection

In this work, reconstructed showers are built geometrically. For an efficient shower separation, in case more than one interaction takes place in the same time slot, a geometric distance D is defined:

$$D_{\alpha,\beta} = \left|\mathrm{plane}_\alpha - \mathrm{plane}_\beta\right| + 2 \times \left(\left|I_\alpha - I_\beta\right| + \left|J_\alpha - J_\beta\right|\right)$$

where α and β label two hits, plane$_\alpha$ is the plane number in which hit α is found, I_α and J_α are the integer coordinate of the hit α in the plane. In each detection plane, there are 96×96 pads. Two adjacent pads will have a difference in I or J equal to 1. The definition of this geometric distance is the result of a study on simulated pion and electron events. It is based on the use of Minimum Spanning Tree algorithm which was successfully applied in the hadron-electron separation study of the CHARM II experiment [6].

The shower reconstruction procedure starts with the first plane containing hits, nearby hits with a distance $D < 15$ are associated to the same reconstructed shower otherwise a new reconstructed shower is created. The iteration then progresses through the GRPC planes, and new hits are added, or new reconstructed showers created. To keep reconstructed showers consistent with physical interaction, and eliminate fake reconstructed showers produced by isolated noise hits the following cuts are applied:

$$N_{\text{hit}} > 25$$

$$\lambda_3 > 4.5 \text{ cm}$$

$$\frac{\lambda_2}{\lambda_3} > 0.01$$

Figure 6 shows the result of the Principle Component Analysis algorithm for a 50 GeV pion and a beam muon in the same event time slot superimposed on the event display of the corresponding event.

3.3 Event selection

3.3.1 Beam and cosmic muon rejection

As can be seen in Fig. 6, tracks have a very small transverse development. A transverse ratio TR is defined as

$TR = \frac{\sqrt{\lambda_1^2+\lambda_2^2}}{\lambda_3}$ where $\lambda_{1,2,3}$ are defined in section 3.1.

Figure 7 shows the distribution of TR for all reconstructed showers for the 7.5 GeV run and for the 60 GeV runs. No selection is applied to the distribution shown except the removal of coherent noise events. A rejection cut at 0.1 removes more than 98 % of the tracks. Figure 8 shows the correlation between TR and the total number of hits for the two different run energies. It can be seen that reconstructed showers with low TR value have a number of hits of the order of twice the number of layers, which is the typical number of hits expected from muon tracks going through the detector.

To further remove cosmics, the number of interaction planes and shower planes are used (see section 3.1 for the definition of interaction and shower planes). To be kept, the events should contain at least three interaction planes. It is also asked that the ratio of the number of interaction planes over the number of shower planes should be greater than 0.5. For a pion shower, almost all shower planes should be interaction planes, and this ratio should be close to 1. On the contrary, for muons, most of the shower planes would not have enough hits to be qualified as interaction planes, and so the ratio should be close to 0.

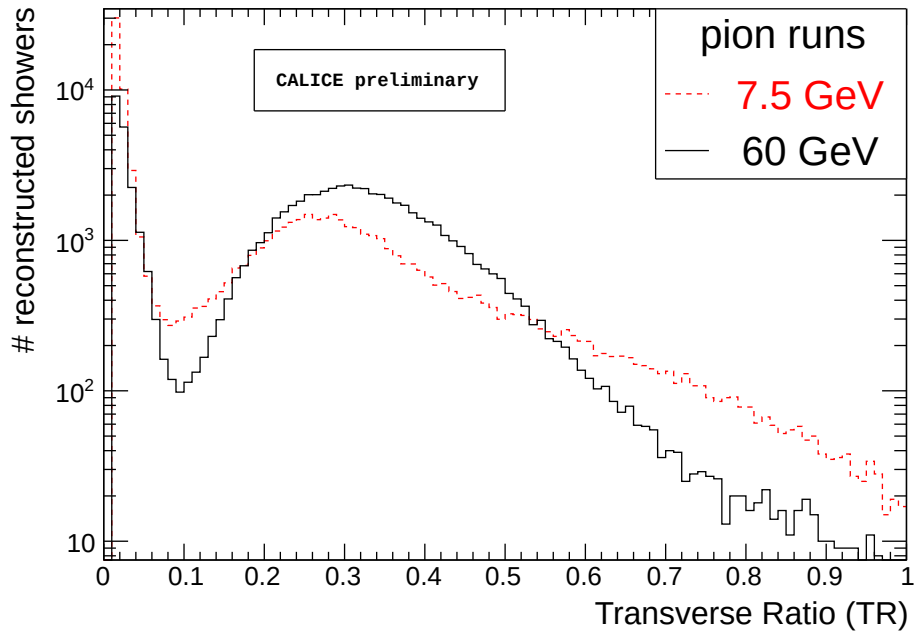

Figure 7. Transverse ratio TR of all reconstructed showers for 7.5 GeV pion run (red dashed line) and for 60 GeV pion runs (black line). The peak at low TR values corresponds to the muon contamination in the pion beam.

3.3.2 Electron rejection

To study the hadronic shower energy resolution, the contamination of the pion samples by electrons should be drastically reduced. The two topological variables introduced in section 3.1 are used to obtain a good e-π separation. To check the power of such variables we show in Fig. 9 scatter plots of the V_1 and V_2 variables for a pion run and an electron run of the same energy (60 GeV). A clear separation can be obtained by using the product of the two variables. A cut of $V_1 \cdot V_2 > 0.045$ separates efficiently the two samples. See Table 1 for cut values for other beam energies.

The same variables are also used to purify the pion samples at low energy where the contamination is rather high (5 GeV and 7.5 GeV runs).

Figure 9 shows also a scatter plot of the V_1 and V_2 variables for the 7.5 GeV pion run. Figure 10 shows the $V_1 \cdot V_2$ product for the same data samples. A cut value of 0.06 is used to select the pion sample. The cut values for the analyzed beam energies are given in Table 1.

pion run energy (GeV)	5	7.5–15	20	30–40	50–60	70–80
min $V_1 \cdot V_2$ value	0.065	0.06	0.055	0.05	0.045	0.04

Table 1. Value of $V_1 \cdot V_2$ used to separate pions from electrons as a function of the nominal pion beam energy.

Using $V_1 \cdot V_2$ variable is a powerful tool to reject electron contamination with almost no loss of pions in particular for pion runs with energies of more than 10 GeV. At lower energies the estimated

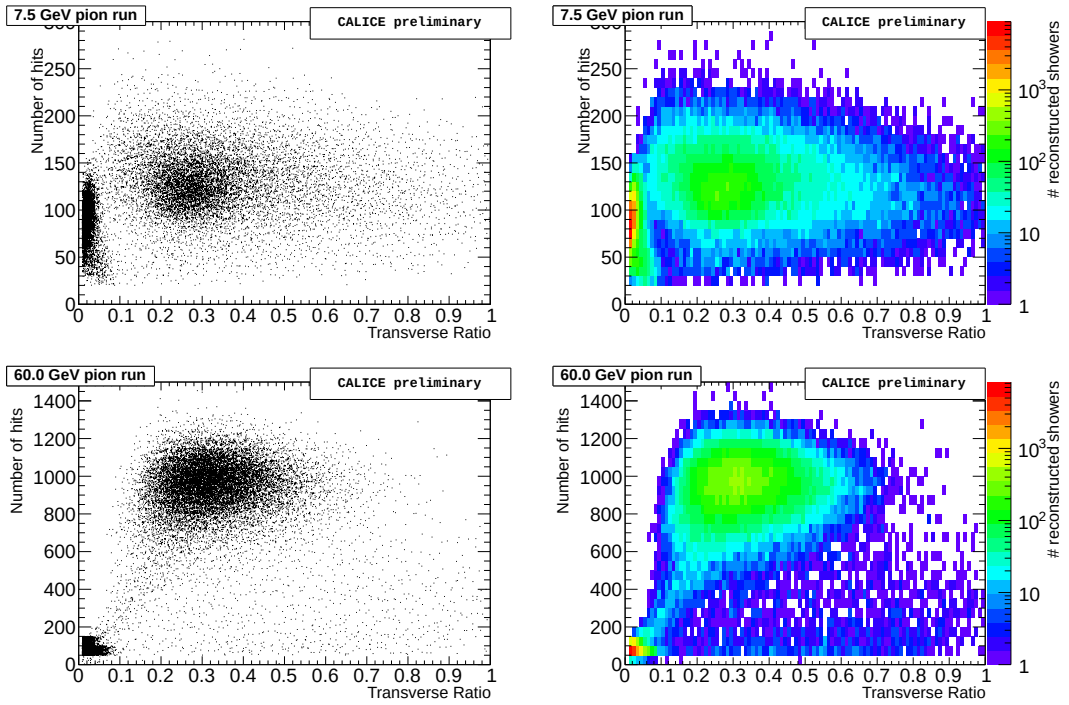

Figure 8. Scatter plots of the number of hit versus transverse ratio for the 7.5 GeV pion run (top) and the 60 GeV pion runs (bottom) for all reconstructed showers in the run. On the right, the same distributions are presented as logarithmic color levels. Notice the difference in vertical scale between the 7.5 GeV run (top) and the 60 GeV runs (bottom).

contamination after using the $V_1 \cdot V_2$ is still low (few percent). To account for this in the following energy resolution study, a variation of this selection cut by 10% is taken as the systematic bias introduced by this cut.

3.3.3 Leakage reduction

To measure more precisely the energy and the resolution of the SDHCAL, a selection of well contained showers is done with the following conditions:

- The first plane of the reconstructed shower containing a hit (but not necessarily an interaction plane) should be one of the first four planes. This cut removes showers induced by cosmics entering laterally in the SDHCAL.
- The first interaction plane should be in the first 15 planes. This removes late interacting hadrons.
- The last shower plane with hits should be before the 42nd plane, or the ratio of the number of hits in the last seven planes to the number of hits in the 30 first ones should be less than 0.15.

The two last conditions favor the selection of events with a shower fully contained in the SDHCAL.

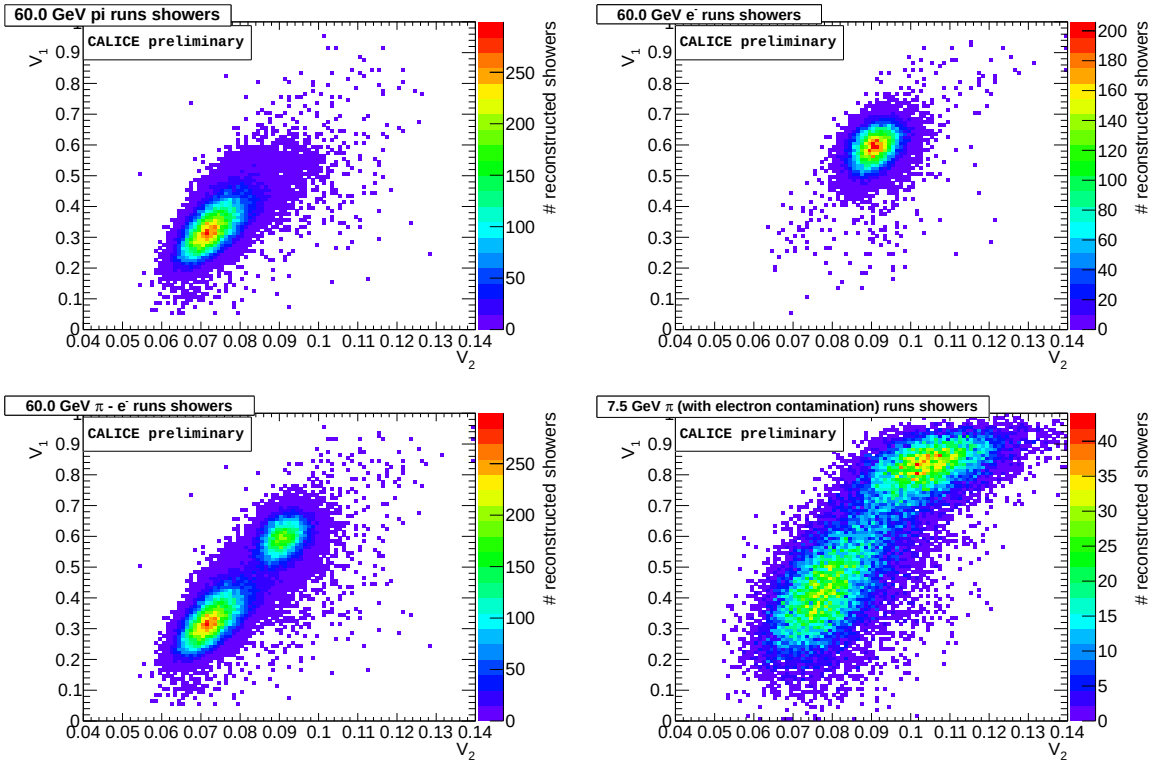

Figure 9. Correlation between V_1 and V_2 for 60 GeV pion runs (top left), 60 GeV electron runs (top right), a mixture of the two sets of runs displayed on top (bottom left) and for the 7.5 GeV pion run (bottom right) which has electron contamination.

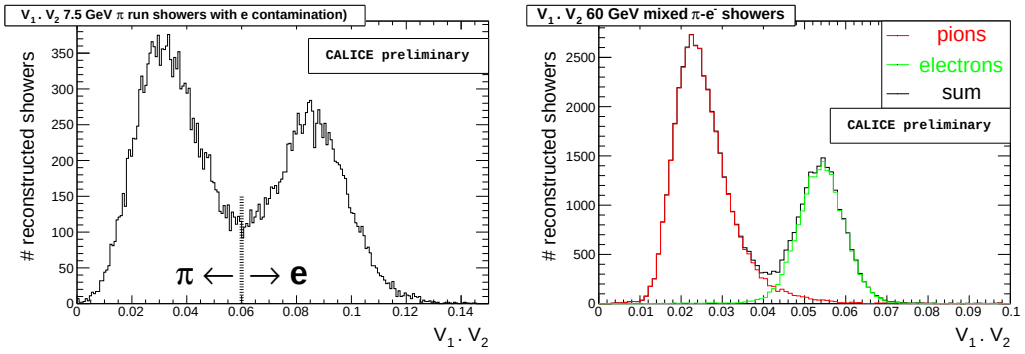

Figure 10. Product of V_1 and V_2 for the 7.5 GeV pion run data (left) and for the 60 GeV pion and electron runs data (right). The 7.5 GeV pion beam was contaminated with electrons while at 60 GeV, it was possible to have pions and electrons separated in different beams. On the left plot, the line shows the cut used to separate pions from electrons.

4. Energy resolution

The selection of hadronic showers based on the criteria presented in the previous section allows to study the linearity and the energy resolution of the hadronic showers measured in the SDHCAL prototype in the running conditions presented in the introduction. The selected hadronic showers belonging to runs of the same energy of both May and August periods were combined by energy (see Table 2), and the distribution of the total number of hits (N_{hit}) is plotted for each energy (see Fig. 11).

Energy [GeV]	Number of reconstructed showers
5	9504
7.5	15074
10	20406
15	33405
20	78391
25	59495
30	53179
40	48720
50	76566
60	38917
70	30893
80	32964

Table 2. Number of selected hadronic reconstructed showers for each energy.

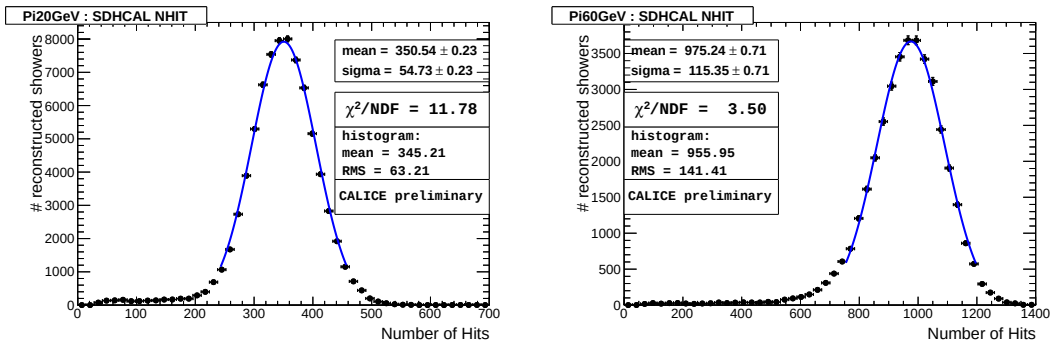

Figure 11. Total number of hits for pion showers of 20 GeV (left) and 60 GeV (right). The distributions are fitted with a Gaussian function in a $\pm 2\sigma$ range around the mean.

Two kinds of fits are used to estimate the average number of hits for a given energy. The first one is using a Gaussian with a fit range limited to two standard deviations around the mean value (Fig. 11). This limitation is due to the tail at low number of N_{hit}. The second fit uses the Crystal Ball (CB) function [7] (see Appendix A for a definition) that was proposed by the collaboration of the same name, to take into consideration the presence of this tail. The Crystal Ball function has

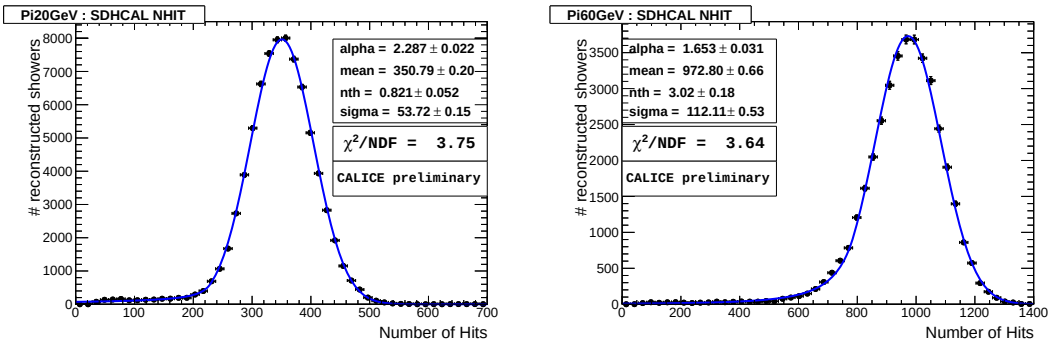

Figure 12. Total number of hits for pion showers of 20 GeV (left) and 60 GeV (right). The distributions are fitted with a Crystal Ball function.

been used also in the work of [8]. Figures 11 and 12 show the distributions of $N_{\rm hit}$ for two different studied energies with the Gaussian and the CB fits respectively.

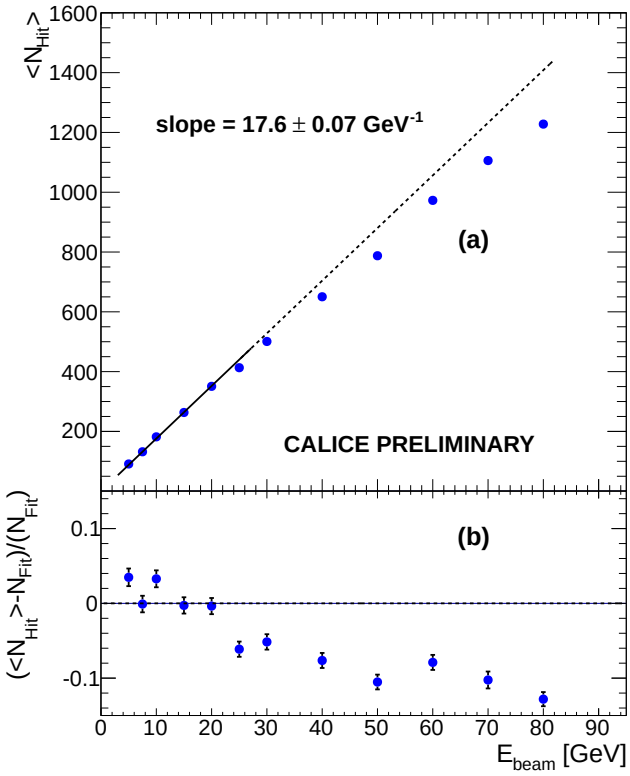

Figure 13. (a) Mean number of hits as a function of the beam energy for reconstructed pion showers. The line indicates the result of a fit that $< N_{\rm hit} >=$slope $\cdot E_{\rm beam}$ made with the first six points (solid section of the line). (b) Relative deviation of the observed mean number of hits to the fitted line shown in (a) as a function of the beam energy for reconstructed pion showers.

The results using the CB fit are summarized in Fig. 13(a). One can see from this plot and

the plot shown in Fig. 13(b) the deviation of the detector response with respect to the straight-line defined by $N_{\rm hit} = 17.6\,E_{\rm beam}$ obtained by fitting the data points between 5 and 25 GeV.

4.1 SDHCAL: Binary mode

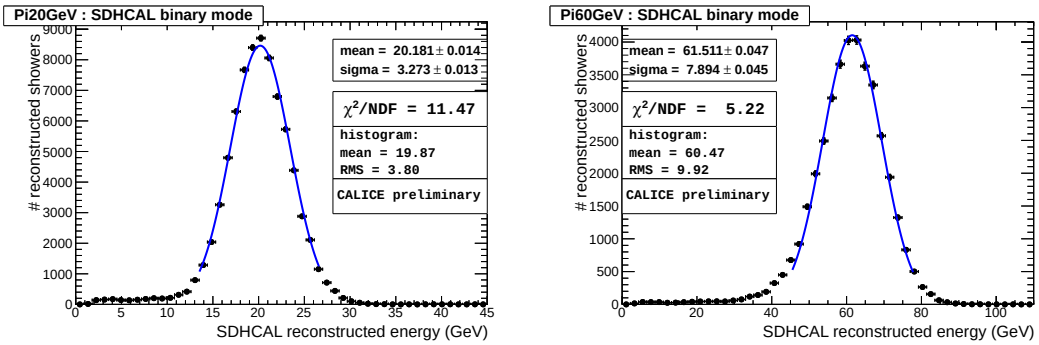

Figure 14. Reconstructed energy for pion showers using only the total number of hits (binary mode with quadratic $N_{\rm hit}$ function). The distributions are fitted with a Gaussian function in a $\pm 2\sigma$ range around the mean. Left is for beam energy of 20 GeV, and right for beam energy of 60 GeV.

The observed behavior of the mean number of hits ($N_{\rm hit}$) as a function of the energy (Fig. 13)(a) suggests that one can find the energy of the hadronic shower up to 20–30 GeV by just weighting the total number of hits by a constant coefficient: $E = C \cdot N_{\rm hit}$ with C determined from the data. For higher energy, the relative deviation of $N_{\rm hit}$ with respect to the value expected from the above simple parametrization shows a rather linear behavior with the beam energy (Fig. 13(b)). This suggests to replace the constant coefficient C by a linear function $(C + D \cdot N_{\rm hit})$. This finally leads to reconstruct the energy with a quadratic function of $N_{\rm hit}$ of the form: $E = (C + D \cdot N_{\rm hit}) \cdot N_{\rm hit}$. Coefficients C and D are then deduced from data, and found to be : $(C = 0.0543,\ D = 0.09 \times 10^{-4})$. The energy distributions obtained in this way are fitted using the same techniques employed for the total number of hits (see Figs. 14 and 15). As expected, this method of shower energy reconstruction restores linearity, as can be seen in Fig. 16. The Crystal Ball fits provide also the Gaussian width, and hence the resolution that one may obtain. Figure 17 shows the relative resolution as a function of the energy. The uncertainty on the resolution is the statistical error increased by the absolute difference of the nominal values found using the two kinds of fits. In addition to this a systematic uncertainty obtained by varying the different selection cuts by 10% around their nominal values were added for the energy reconstruction algorithm linearity and resolution studies for both the binary and the multi-threshold modes.

4.2 SDHCAL: Multi-threshold mode

To fully exploit the data provided by the SDHCAL, the information related to the three thresholds can be used. As mentioned in the introduction this information may help to better estimate the total number of tracks produced in a hadronic shower. Indeed, pads crossed by two particles in the same time window of 200 ns, and separated by a distance larger than that of the avalanche size (1–2 mm) [9] will have their induced charge added. The MIP charge spectrum of the GRPC

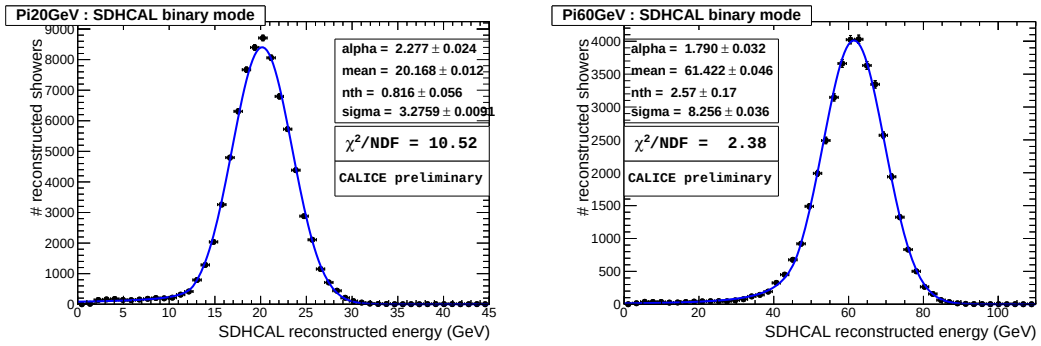

Figure 15. Reconstructed energy for pion showers using only the total number of hits (binary mode with quadratic N_{hit} function). The distributions are fitted with a Crystal Ball function. Left is for beam energy of 20 GeV, and right for beam energy of 60 GeV.

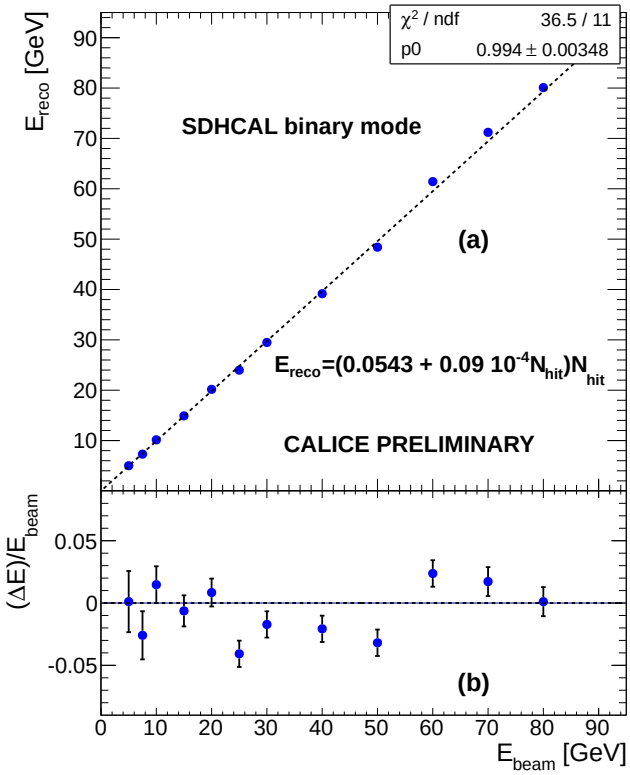

Figure 16. (a) Mean reconstructed energy for pion showers as a function of the beam energy and (b) Relative deviation of the pion mean reconstructed energy relative to the beam energy as a function of the beam energy. The reconstructed energy is computed using only the total number of hits (binary mode with quadratic N_{hit} function).

being broad, the precise measurement of the charge cannot indicate the exact number of charged particles crossing the pad. However it can help to indicate whether this number is low, large or very large. The simulation of hadronic showers in the GRPC-SDHCAL using a realistic GRPC

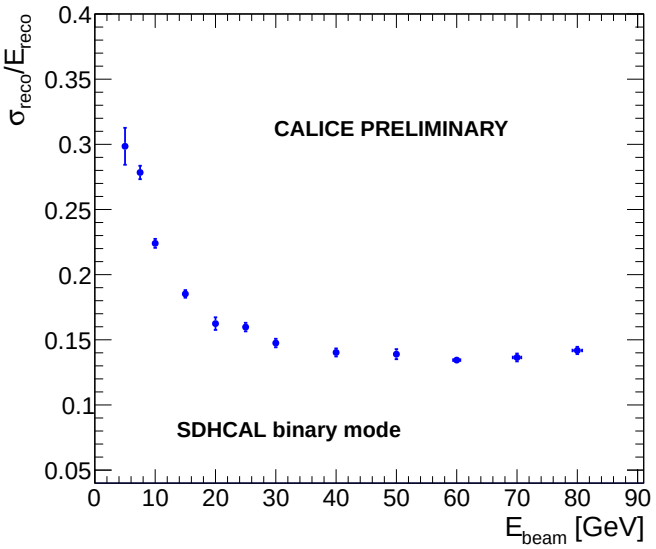

Figure 17. $\frac{\sigma(E)}{E}$ of the reconstructed pion energy E as a function of the beam energy. The reconstructed energy is computed using only the total number of hits (binary mode with quadratic N_{hit} function).

response corroborates this idea. The first validation of this idea is the observation in the hadronic and electromagnetic showers that in the core of the showers, where more particles are expected, a higher density of hits with the second and the third thresholds crossed is observed as can be seen from the event displays of Figs. 18 and 19.

The thresholds information can be useful to understand the shower structure as suggested by these event displays. Nevertheless here this will be used only to improve the energy measurement by expressing the energy of the hadronic shower as a weighted sum of N_1 : the number of hits for which only the first threshold is crossed, N_2 : the number of hits for which both the first and the second but not the third thresholds are crossed, and finally N_3 : the number of hits with the three thresholds crossed. In Fig. 20, the average value of N_1, N_2, N_3 and of the total number of hits of the selected hadronic reconstructed showers are shown.

Taking an empirical approach, the weighted sum can be given by:

$$E_{\text{rec}} = \alpha N1 + \beta N2 + \gamma N3.$$

The complexity of the hadronic shower structure and its evolution with energy do not allow to have constant values of α, β and γ for a large energy range. To overcome this difficulty α, β and γ are parametrized as functions of the total number of hits ($N_{\text{hit}} = N1 + N2 + N3$). This parametrization is possible since the total number of hits is an available information. To find the best parametrization, a χ^2-like expression was used for the optimization procedure on a subset of the data (about third of the 10, 20, 30, 40, 50 and 60 GeV data).

$$\chi^2 = \Sigma_{i=1}^{N} \frac{(E^i_{\text{true}} - E^i_{\text{rec}})^2}{E^i_{\text{true}}}$$

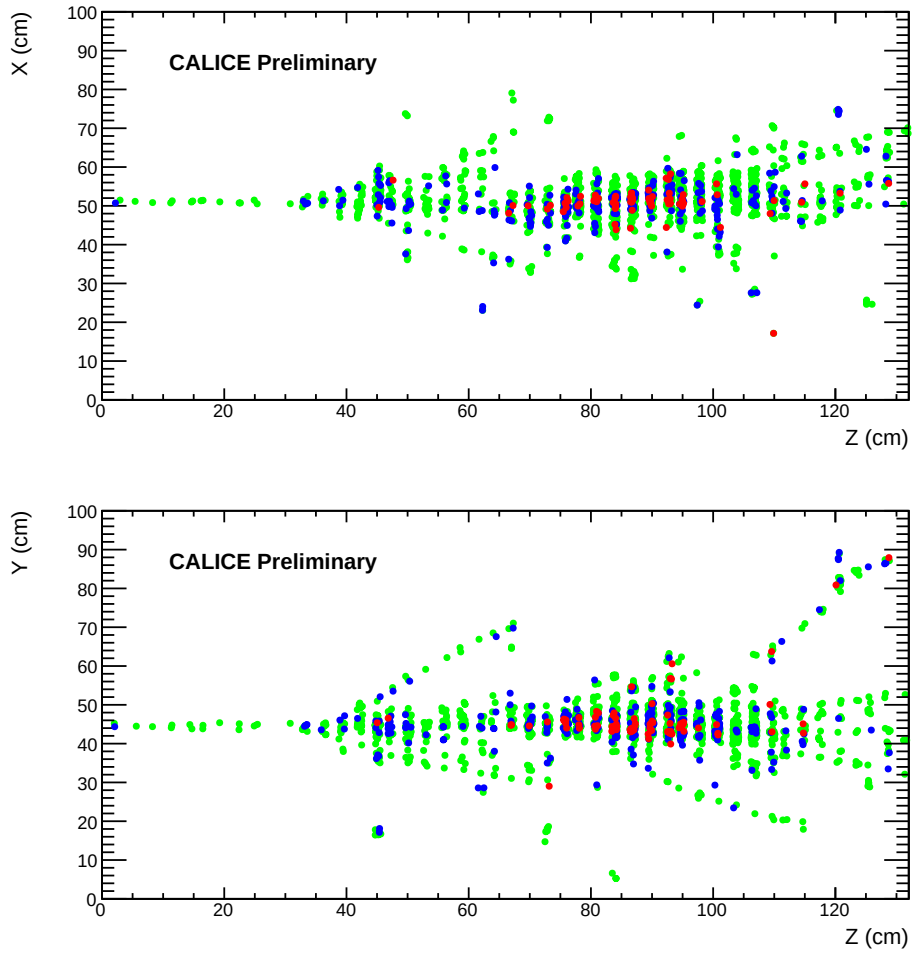

Figure 18. An 80 GeV pion event display with red color indicating highest threshold fired pads, blue color indicating the middle threshold, and green one that of the lowest one.

where N is the number of events used for the optimization. Different functions of $N_{\rm hit}$ were tested to parametrize the evolution of α, β and γ with $N_{\rm hit}$. A polynomial function of second degree was found to give the best results for all three of them. In Fig. 21, the parametrizations of α, β and γ as a function of $N_{\rm hit}$ are presented.

It is worth mentioning here that these parametrizations are not unique, and other parametrizations could be more adequate. It is also very important to recognize that this kind of correction, non-linear in energy, should be applied by principle only at the single particle level once the contribution of each particle and its nature (hadron, electron, ...) are determined. This has been done in this work using topological variables as described above.

The three coefficients of these polynomial functions are then used to estimate the energy of all collected data without using the information of the true energy. The energy distributions obtained in this way are then plotted and fitted as before using both the Gaussian and the CB fits, and are shown in Figs. 22 and 23. As expected, this method of pion shower energy reconstruction restores linearity

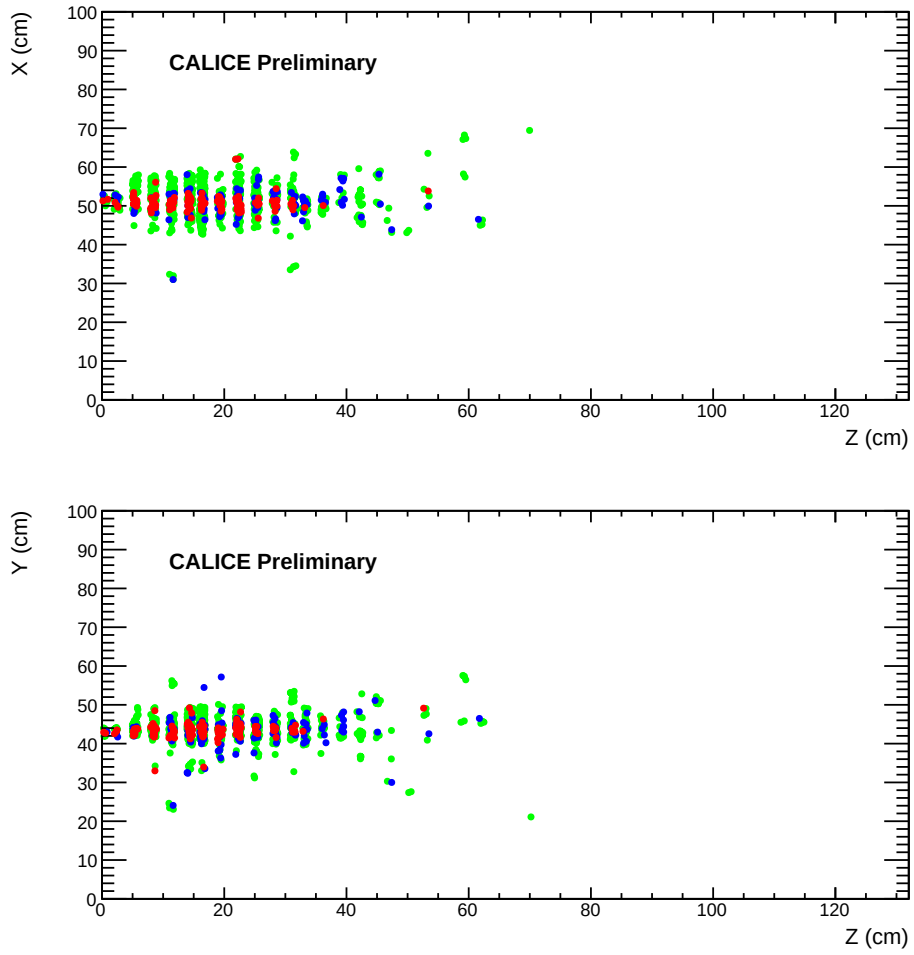

Figure 19. A 70 GeV electron event display with red color indicating highest threshold fired pads, blue color for the middle threshold, and green for the lowest one.

on a large energy scale going from 10 GeV up to 80 GeV as is shown in Fig. 24(a). Figure 24(b) shows the relative deviation of the reconstructed energy with respect to the beam energy.

The use of the three thresholds information has a very good impact on the energy resolution (Fig. 25) at energies higher than 30 GeV as was predicted from our preliminary simulation studies [10]. The energy resolution reaches the value of 9.5% at 80 GeV which is an encouraging result since the used data were collected without any correction to improve the homogeneity of the detector's response.

4.3 Multi-threshold vs. binary modes

Energy reconstruction algorithms using quadratic functions of the total number of hits have been developed both for the binary and the multi-threshold modes of our prototype. Although these algorithms restore linearity over a large energy range, the energy resolution achieved with the binary mode falls behind that with the multi-threshold mode for energies higher than 30 GeV. A

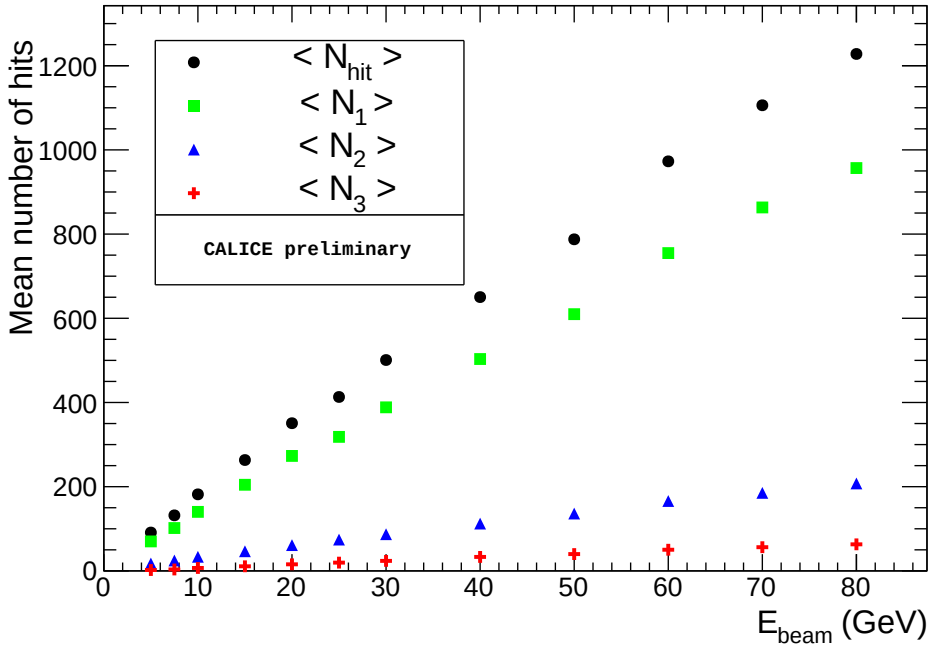

Figure 20. Average number of hits in the hadronic shower sample corresponding to the first threshold only (green squares), to the second threshold but not the third one (blue triangles), to the third threshold (red crosses), and to the total number (black circles) as as a function of the beam energy.

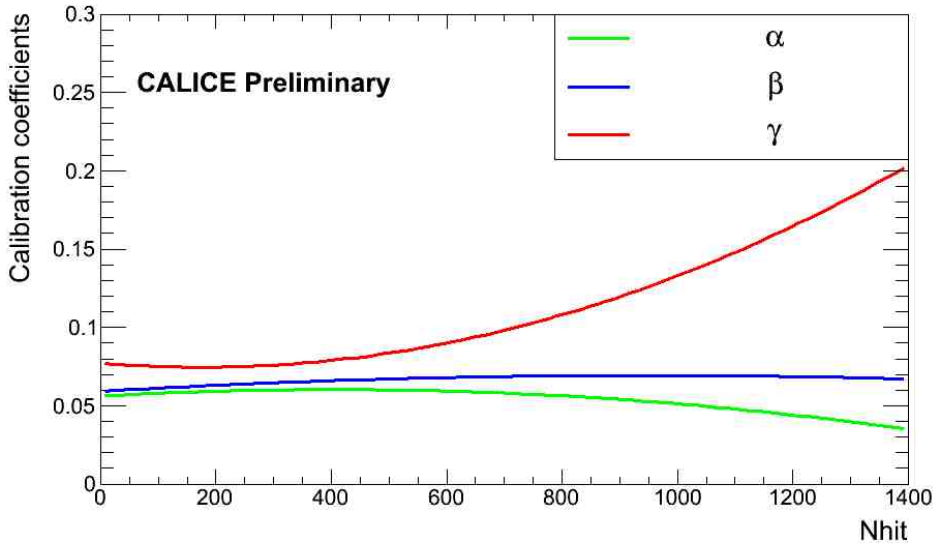

Figure 21. Evolution of the coefficient α (green), β (blue) and γ (red) in terms of the total number of hits.

direct comparison of the two results is shown in Fig. 26. To further compare the two results, the

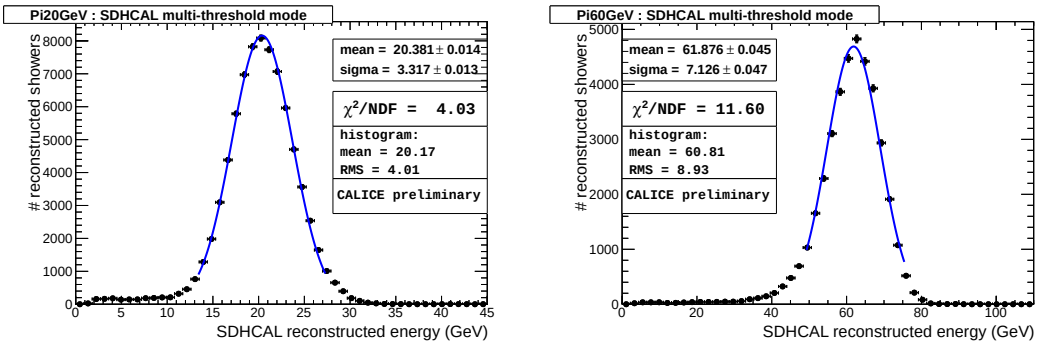

Figure 22. Reconstructed energy for pion showers using information from the three thresholds (multi-threshold mode with energy reconstruction described in section 4.2). The distributions are fitted with a Gaussian function in a $\pm 2\sigma$ range around the mean. Left is for beam energy of 20 GeV, and right for beam energy of 60 GeV.

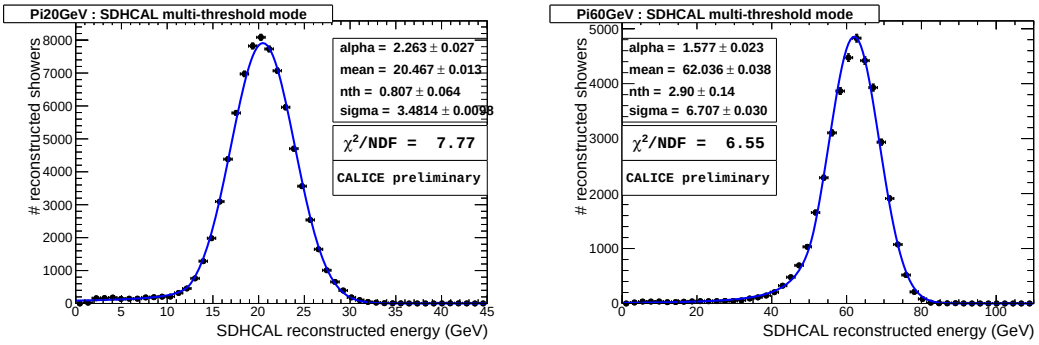

Figure 23. Reconstructed energy for pion showers using information from the three thresholds (multi-threshold mode with energy reconstruction described in section 4.2). The distributions are fitted with a Crystal Ball function. Left is for beam energy of 20 GeV, and right for beam energy of 60 GeV.

reconstructed energy distribution is shown for both modes on Fig. 27 for 80 GeV, 70 GeV and 20 GeV pions. At 70 GeV and 80 GeV, the difference in resolution between the two modes is the most important, and this difference is visible on the energy distribution. At low energy, the two results have similar resolution and similar reconstructed energy distribution as is illustrated by the distributions for the 20 GeV pions on Fig. 27. The linearity achieved with the binary mode seems better at very low energy (5, 7.5 GeV) but this is probably related to the fact that the multi-threshold mode algorithm parametrization has been tuned for energies higher than 10 GeV. For both modes at low energy, a small remaining contamination of the pion sample by electrons may worsen the energy reconstruction resolution. This contamination should be eliminated in order to estimate correctly the resolution of both modes in our SDHCAL prototype. A Cherenkov detector should be added in the future test beam to obtain a pion sample with a better purity.

This resolution improvement at high energy does not mean that a binary mode capable hadronic calorimeter is less performant than the SDHCAL with its multi-threshold mode. It only means that at this stage of our study the thresholds information seem to provide additional information to cor-

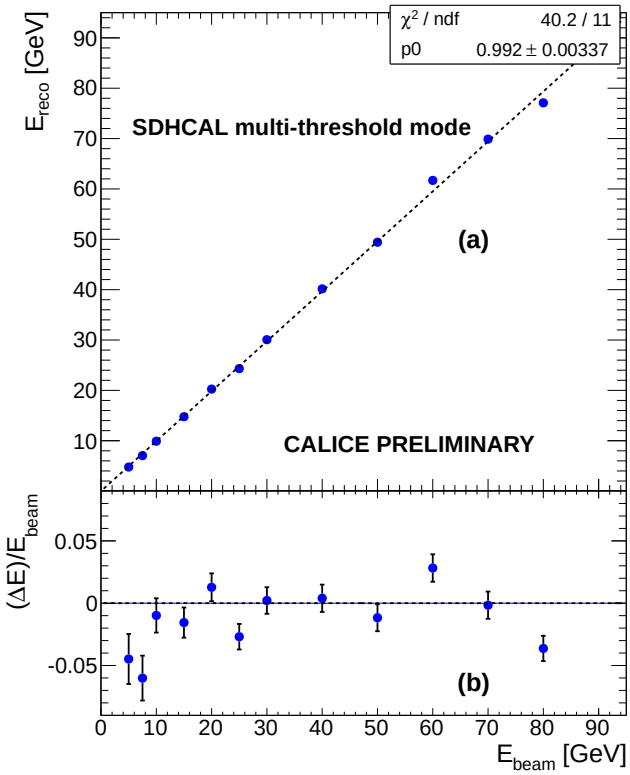

Figure 24. (a) Mean reconstructed energy for pion showers and (b) Relative deviation of the pion mean reconstructed energy with respect to the beam energy as a function of the beam energy. The reconstructed energy is computed using the three thresholds information (multi-threshold mode). The energy is reconstructed with the linearity-restoring algorithm described in section 4.2.

rect for the saturation which starts to show up at energies higher than 30 GeV. In any case the threshold information could improve our understanding of the hadronic shower behavior.

5. Conclusion

The results obtained with the SDHCAL prototype during the 2012 test beam runs using the triggerless, power-pulsing mode seem to be of good quality. Algorithms to linearize the calorimeter response and convert it to energy were developed. They provide 3–4% precision when applied to the raw data. The resolution associated to the linearized energy response of the same selected data sample was estimated in both the binary and the multi-threshold modes. The multi-threshold capabilities of the SDHCAL at high energy (>30 GeV) improve clearly the resolution. This improvement which reaches 30% at 80 GeV is probably related to a better treatment of the saturation effect thanks to the information provided by the second and third thresholds.

Further work is needed to confirm this result. This can be done in particular using an ongoing simulation study. This will help to thoroughly understand the mechanism behind this improvement, and leads to a better selection of the threshold values for the future.

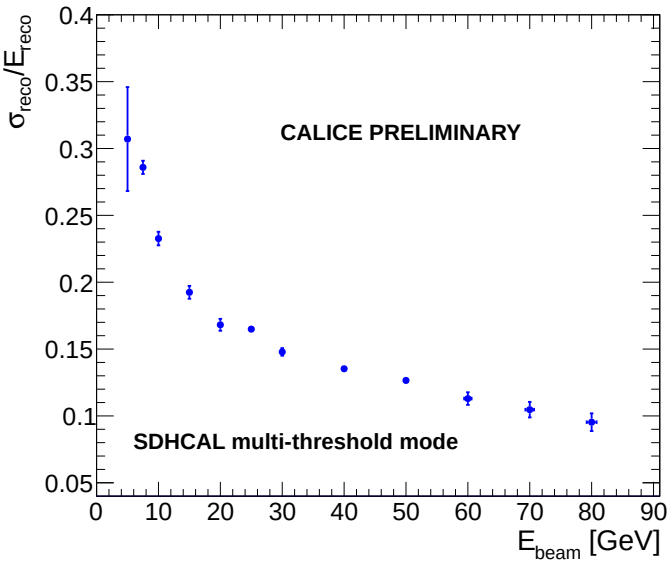

Figure 25. $\frac{\sigma(E)}{E}$ of the reconstructed pion energy E as a function of the beam energy. The reconstructed energy is computed using the three thresholds information (multi-threshold mode), and the distributions are fitted with a Crystal Ball function. The energy is reconstructed with the linearity-restoring algorithm described in section 4.2.

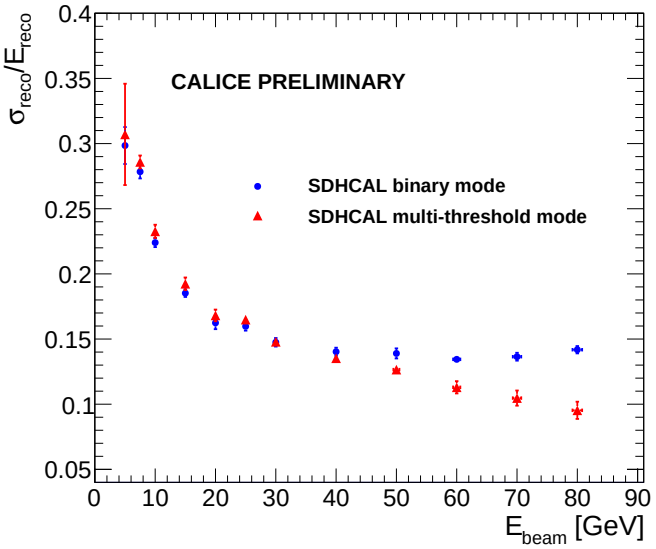

Figure 26. $\frac{\sigma(E)}{E}$ of the reconstructed pion energy E as a function of the beam energy. For the blue circles graph, the reconstructed energy is computed using only the total number of hits (binary mode). For the red triangles graph, the reconstructed energy is computed using the three thresholds information (multi-threshold mode). For both modes, the energy is reconstructed using quadratic functions of the total number of hits.

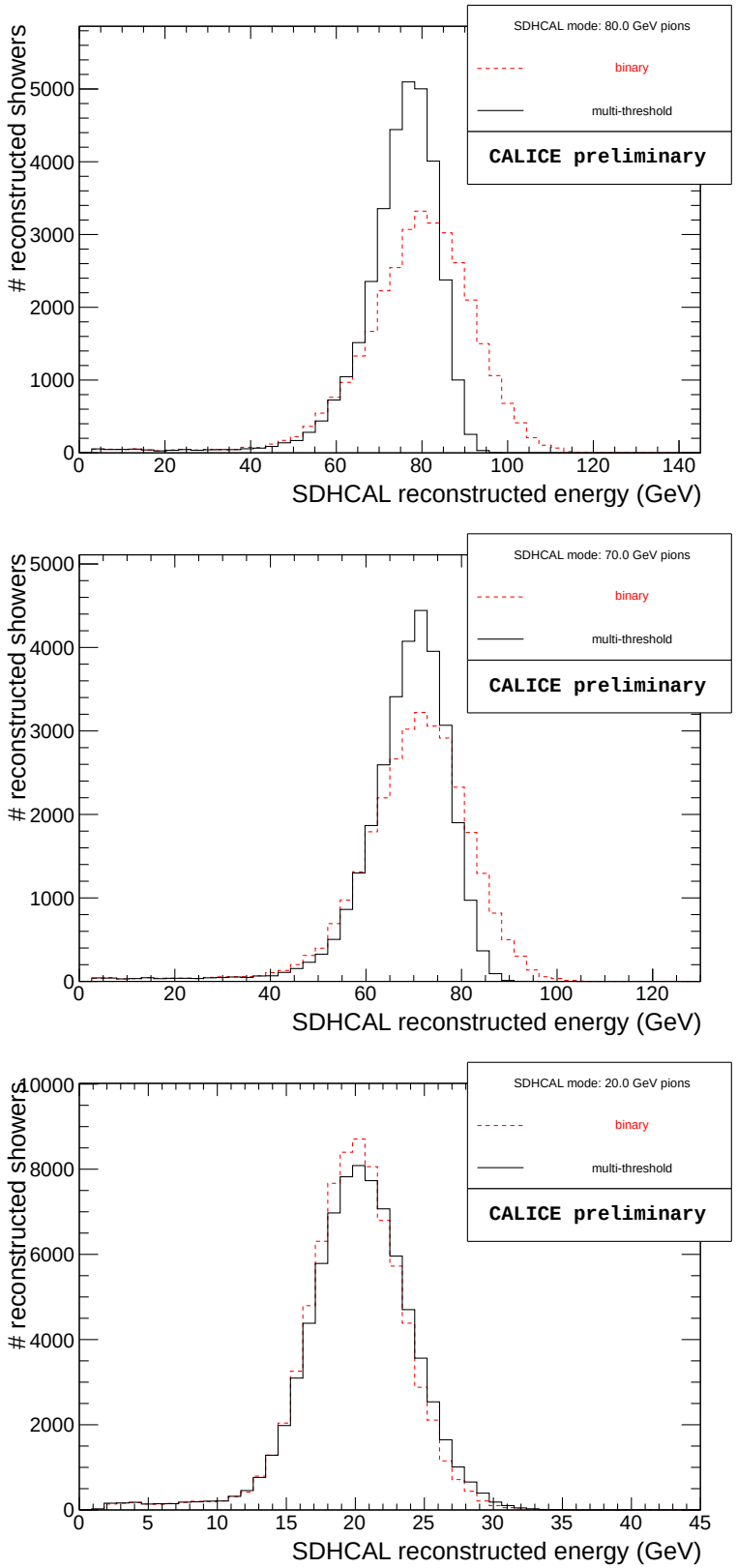

Figure 27. Distribution of the reconstructed energy with the SDHCAL binary mode (red dashed line), and with the SDHCAL multi-threshold mode (solid black line) for pions of 80 GeV (top), 70 GeV (middle) and 20 GeV (bottom).

References

[1] F. Dulucq *et al.*, *HARDROC: Readout chip for CALICE/EUDET Digital Hadronic Calorimeter*, Nuclear Science Symposium Conference Record (NSS/MIC), 2010 IEEE, pp.1678-1683, Oct. 30 2010-Nov. 6 2010 doi: 10.1109/NSSMIC.2010.5874060

[2] B. Bilki *et al.*, *Measurement of the rate capability of Resistive Plate Chambers*, *JINST* **4** P06003

[3] E. Abat *et al.*, *Study of energy response and resolution of the ATLAS barrel calorimeter to hadrons of energies from 20 to 350 GeV*, NIM A, Volume 62, Issues 1-3, 1-21 September 2010.

[4] K. Pearson, *On Lines and Planes of Closest Fit to Systems of Points in Space*, Philosophical Magazine 2 (11), 1901, pp 559-572.

[5] M. Ruan *et al.*, *Fractal dimension analysis in a highly granular calorimeter*, J. Phys. Conf. Ser. 368 (012038).

[6] K. Winter *et al.*, *An electron-hadron separation for digital sampling calorimeters*, CHARM II Collaboration, CERN-EP/88-87, 26 July 1988.

[7] J. E. Gaiser, *Charmonium Spectroscopy from Radiative Decays of the J/Ψ and Ψ'*, SLAC-R-255, PhD thesis, Stanford University, Stanford, California 94305, 1982

[8] Y. Karyotakis *et al.*, *Analysis of the May 2012 test beam data with the SDHCAL*, CALICE Internal Note CIN-019

[9] Y. Qian *et al.*, *Measurement of avalanche size and position resolution of RPCs with different surfaces resistivities of the high voltage provider*, CPC (HEP & NP), 2010, vol.34, pp 565-570.

[10] S. Mannai, *Energy Reconstruction in GRPC Semi-Digital HCAL*, talk given at CALICE collaboration meeting, September 16-18 2009, Lyon, France (`http://ilcagenda.linearcollider.org/getFile.py/access?contribId=16&sessionId=1&resId=1&materialId=slides&confId=3642`)

A. Crystal Ball function

The Crystal Ball function[7], named after the Crystal Ball Collaboration, is a probability density function that can be used to model a detector Gaussian response with low-end tails related to loss of information usually due to saturation of a portion of the detector. It consists of a Gaussian core portion and a power-law low-end tail, below a certain threshold. The function itself and its first derivative are both continuous. The Crystal Ball function is given by:

$$f(x;\alpha,nth,\bar{x},\sigma) = N \cdot \begin{cases} \exp(-\frac{(x-\bar{x})^2}{2\sigma^2}) & \text{for } \frac{x-\bar{x}}{\sigma} > -\alpha \\ A \cdot (B - \frac{x-\bar{x}}{\sigma})^{-nth} & \text{for } \frac{x-\bar{x}}{\sigma} \leq -\alpha \end{cases} \tag{A.1}$$

where:

$$A = \left(\frac{nth}{|\alpha|}\right)^{nth} \cdot \exp\left(-\frac{|\alpha|^2}{2}\right) \tag{A.2}$$

$$B = \frac{nth}{|\alpha|} - |\alpha| \tag{A.3}$$

N is a normalization factor.

B. Observed resolution

The following table lists the resolution observed as plotted in Figs. 17 and 25.

Energy (GeV)	binary mode	multi-threshold mode
5	0.298 ± 0.014	0.31 ± 0.04
7.5	0.278 ± 0.005	0.286 ± 0.005
10	0.224 ± 0.003	0.233 ± 0.005
15	0.185 ± 0.003	0.192 ± 0.004
20	0.162 ± 0.005	0.168 ± 0.002
25	0.160 ± 0.003	0.165 ± 0.003
30	0.148 ± 0.003	0.149 ± 0.002
40	0.140 ± 0.003	0.135 ± 0.002
50	0.139 ± 0.004	0.127 ± 0.005
60	0.134 ± 0.001	0.113 ± 0.006
70	0.136 ± 0.003	0.105 ± 0.007
80	0.142 ± 0.003	0.095 ± 0.004